# Ultrasonic and microstructural evaluation of cemented paste backfill properties containing alkali-activated slag: Effect of slag fineness

Ferdi Cihangir * and Ercument Koc

Posted Date: 2 November 2023

doi: 10.20944/preprints202311.0116.v1

Keywords: Cemented paste backfill; alkali-activated slag; slag fineness; ultrasonic pulse velocity; microstructure; durability

*Article*

# Ultrasonic and Microstructural Evaluation of Cemented Paste Backfill Properties Containing Alkali-Activated Slag: Effect of Slag Fineness

**Ercument Koc [1] and Ferdi Cihangir [2,*]**

[1] Department of Metallurgical and Materials Engineering, Ataturk University, Erzurum, Turkey; *ercument.koc@atauni.edu.tr*

[2] Department of Mining Engineering, Karadeniz Technical University, Trabzon, Turkey

* Correspondence: cihangir@ktu.edu.tr; Tel.: (+904623774055)

**Abstract:** Cement paste backfill (CPB) is an effective waste management method allowing the storage of fine process tailings into underground mined-out voids. CPB performance generally depends on the sulfur content of the tailings and the type of binder. In recent years, there has been an increasing trend on the use of alkali-activated slag (AAS) to improve the performance properties of CPB. This study focuses on the ultrasonic and microstructural investigation of the effect of slag fineness on the mechanical, geochemical and durability properties of CPB made up of AAS (AAS-CPB) over 360 days. In this scope, AAS-CPB samples were prepared at three different fineness (3100-4650-6300 $cm^2/g$). Fineness of slag significantly improved the early age- and long-term strength (~2.3 fold and ~6.6 fold, respectively) of CPB. However, further increase of slag fineness may have adverse effect on CPB microstructure and strength in the long term. Ultrasonic pulse velocity monitoring displayed very high relation with the strength evolution and durability assessment of CPB. Slag fineness at a degree was seen to improve the pore structure evolution of AAS-CPB. Microstructural studies are in good agreement with the geochemical and durability behavior of AAS-CPB. Microstructural and ultrasonic findings suggest that while slag fineness enhances the mechanical properties of AAS-CPB, further increase of the fineness of slag has no additional important technical advantages.

**Keywords:** cemented paste backfill; alkali-activated slag; slag fineness; ultrasonic pulse velocity; microstructure; durability

## 1. Introduction

The development and growth of the global economies and the investments in technological studies increase the need for underground raw materials day by day. The increasing need for raw materials entails deeper open pit mining or underground mining operations. In most cases, extracted ores from the earth's crust necessitate fine grinding and chemical treatments to gain such raw materials/precious metals etc. As a result, large amounts of fine processed tailings are produced which may contain environmentally hazardous compounds (Chen et. al. 2018; Koc et. al. 2023).

Environmentally friendly management of these kind of tailings/wastes is of great importance. Such materials are mostly stored in tailings dam or placed into underground mining voids as cemented paste backfill (CPB). Tailings dams require large areas and constant maintenance, and carry high risks against collapses. On the other hand, the use of CPB technology has been increasing and becoming widespread all over the world in the last 40 years and especially in recent years for the management of these tailings (Chen et. al. 2019; Koc et. al. 2023; Meng et. al. 2023).

CPB is widely used as a combination of cut and fill underground mining method. It provides many environmental and technical advantages, safe working conditions, providing high mining cycle, increasing ore gain rate and mine life, decrease the mining cost, etc. (Chen et. al. 2022; Wu et.al. 2020; Kasap et. al. 2022; Pan and Grabinsky, 2023).

CPB is a successfully designed engineering cemented material and prepared using fine processing tailings, water and cement agents. Performance properties of CPB is very significant

 doi:10.20944/preprints202311.0116.v1



during its service life. Strength, durability and consistency are among the most important properties of CPB. Therefore, characterization of each component is very important. Up to day, binder types and dosages (Kesimal et. al. 2003; Ercikdi et. al. 2009a; Cihangir et. al. 2015), physical, mineralogical and chemical properties (Benzaazoua et. al. 1999; Kesimal et. al. 2003; Fall et. al. 2005; Liu et. al. 2020), microstructural, workability, and rheological properties (Clayton et. al. 2003; Kesimal et. al. 2004; Annor et. al. 2006; Ercikdi et. al. 2009b; Cihangir and Akyol, 2020), durability properties (Cihangir et. al. 2015; Cihangir et al. 2018) of CPB were extensively studied.

Interaction of binder agent and tailings is very important for CPB performance (Benzaazoua et al. 2004). Therefore, each tailings entails special design in case of the use as CPB material for the desired strength, durability and consistency. In most cases, CPB has 30-50% porosity, 15-30% moisture. Based on the strength requirements, 5-10 wt.% binder is used in general. Tailings can contain high amount of sulphidic minerals such as pyrite. In case of air and water, pyrite minerals oxidize and generate acid and sulphate products.

Ordinary Portland cement is the most common binder used in CPB applications. However, it is vulnerable to acid and sulphate effects due to the instrinct properties such as high CaO and $C_3A$ content (Ercikdi et. al. 2009a,b; Cihangir et. al. 2012; Ercikdi et. al. 2013). Therefore, have been extensive studies to overcome this problem and produce durable CPB material (Ercikdi et al. 2010a,b; Cihangir et. al. 2012; Pokharel and Fall, 2013). Durability of CPB is followed by unconfined strength tests. Besides, geochemical and microstructural properties are other main factors for durability assessments. Recently, there has been an increasing interest in the use of alkali-activated slag cements (AAS) for CPB preparation to increase the quality and microstructural properties of CPB. In this scope, slag and activator type (Cihangir et al. 2012-2015), tailings type and activator design (Cihangir et. al. 2018), strength, workability and rheological properties (Xue et. al. 2018; Cihangir and Akyol 2020; Kou et al. 2020; Jiang et. al. 2020) were studied. Among these Cihangir and his team investigated the durability of CPB prepared using AAS in the long-term. However, the effect of slag fineness on the mechanical, microstructural and durability properties of sulphide-rich tailings CPBs produced with alkali-activated slag was not investigated in the long term (360-days).

On the other hand, ultrasonic P-wave velocity (ultrasonic pulse velocity:UPV) test was used recently for the prediction of UCS of CPB. UPV test is an efficient and non-destructive method sensitive to the bond strength, compactness of the materials, structural defects etc. indicating the quality of solid materials (Altindag, 2012). Physical, mechanical and geotechnical properties can be determined via UPV test (Kilic and Teymen, 2008; Altindag, 2012; Karaman and Kesimal, 2013). Besides, UPV is very sensitive to weathering properties, heterogeneity, cracks etc. in rock material (Karpuz and Pasamehmetoglu, 1997; Hamdi and Lafhaj, 2013), and therefore, UPV provides quality control solutions for material classifications (Christaras, 2009).

As for CPB, previous studies investigated only the short-term relations between UCS and UPV of cemented paste backfill samples up to 7 days (Wu et al. 2018), 14 days (Yan et al. 2020), 28 days (Wu et. al. 2016; Qiu et. al. 2020; Xu. et. al. 2021) and 56 days (Ercikdi et al., 2014; Xu et al., 2017; Jiang et. al. 2020; Yilmaz et al., 2014; Yilmaz and Ercikdi, 2016), 90 days (Jiang et al. 2020; Sari et. al. 2023) of curing periods. However, no study was carried out for the durability assessment of CPB via UPV in the long term together with detailed microstructural properties of CPB.

Therefore, this is the first study aiming the investigation of the effect on slag fineness and its use as alkali-activated binder on the mechanical, geochemical, microstructural and durability properties of CPB. Since UPV is a very sensitive and strong tool for the determination of structural defects, it was also firstly used for the durability assessment of CPB produced with AAS using slags at different fineness in the long term.

## 2. Materials Characterization and Experimental Studies

### *2.1. Characterization of tailings and binders*

Sulphide rich tailings for this study was obtained from a copper-zinc plant located in the northwest of Turkiye. Tailings was taken from the disc filter outlets in the paste backfill plant and

Preprints (www.preprints.org) | NOT PEER-REVIEWED | Posted: 2 November 2023 doi:10.20944/preprints202311.0116.v1



brought to the laboratory. After the homogenization, particle size distribution (PSD) of the tailings was measured under laser diffraction method with a Malvern Mastersizer Hydro 2000 MU (Figure 1a). Water is used as dispersing medium and ultrasound was also utilized to better disperse the particles. Considering $C_u$ (coefficient of uniformity) and $C_c$ (coefficient of curvature) values (Table 1), the tailings material has a well particle size distribution (Annor et al. 2006). It is a medium sized material with a fine particle content about 48.85% under 20 micron ((Landriault, 2001).). Fineness of the tailings was determined according to TS EN 196-6 (2010) in a cement plant located in Trabzon/Turkiye. Specific gravity was determined in accordance with ISRM (2007).

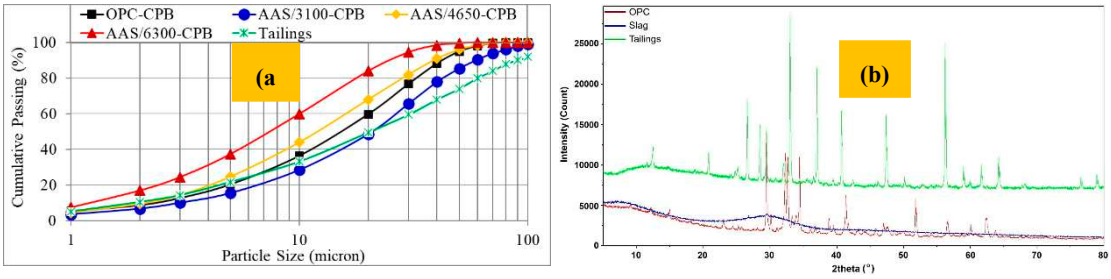


**Figure 1.** Particle size distributions (a) and XRD profiles (b) of the materials.

**Table 1.** Chemical, physical and mineralogical properties of the tailings.

| Chemical composition (%) | Value | Physical properties | Value | Mineralogical Content (%) | Value |
|---|---|---|---|---|---|
| $SiO_2$ | 15.24 | Specific gravity | 3.95 | Quartz | 15.4 |
| $Al_2O_3$ | 3.69 | Specific surface ($cm^2/g$) | 3066 | Pyrite | 56.3 |
| $Fe_2O_3$ | 49.19 | -20μm material content (%) | 48.85 | Clinochlore | 4.5 |
| CaO | 2.56 | $D_{10}$ (μm) | 1.84 | Kaolinite | 3.1 |
| MgO | 1.64 | $D_{30}$ (μm) | 8.44 | Calcite | 4.6 |
| $TiO_2$ | 0.21 | $D_{50}$ (μm) | 20.97 | Amesite | 4.1 |
| $Cr_2O_3$ | 0.03 | $D_{60}$ (μm) | 30.37 | Siderite | 2.0 |
| $Na_2O$ | 0.98 | $D_{90}$ (μm) | 90.37 | Dolomite | 2.4 |
| $K_2O$ | 0.22 | $C_u$ | 16.51 | Acmite | 1.0 |
| MnO | 0.07 | $C_c$ | 1.27 | Copiapite | 1.0 |
| $P_2O_5$ | 0.06 | Initial pH | 8.98 | Hematite | 2.7 |
| Loss on ignition | 23.30 | Initial $SO_4^{2-}$ (ppm) | 5712 | Halloysite | 0.8 |
| $S^{2-}$ (Sulphide) | 32.33 | | | Gypsum | 1.0 |
| Total S | 28.89 | | | Others | ~1.1 |

$C_u$: ($D_{60}/D_{10}$); $C_c$: ($(D_{30})^2/(D_{10}\times D_{60})$).

Chemical analysis of the tailings was performed at ACME laboratories in CANADA using X-ray fluorescence (XRF) (Table 1). X-ray diffraction (XRD) analyses was carried out using a **Panalytical X'Pert3 Powder model machine equipped with a** Pixel 1D detector in Karadeniz Technical University Central Research Laboratories (KTU-CRL). Analyze duration is 1 h for each sample between 5–80° under 2θ with a 0.013° step size. Scanning rate was applied as 1.25° per minute for reliable determination of the crystalline phases of the materials (Figure 1b). Under these conditions, Rietveld technique was conducted for the determination of mineralogical contents (Table 1). As can be seen from Table 1, pyrite is the dominant mineral.

Ordinary Portland cement (OPC: CEM I 42.5R) was obtained from a cement company in Trabzon/Turkiye. Slag was taken from an iron-steel slag plant as water quenched material and grinded in the laboratory to prepare slags having different specific surface area (SSA:fineness). Chemical, physical and mineralogical analyses were performed together with the tailings under same

 doi:10.20944/preprints202311.0116.v1



standards/methods at the same laboratories mentioned above. According to the chemical composition, slag has an acidic character with a basicity index (BI) value of 0.96. BI value was calculated using the formula suggested by Bauné et al. (2000). Pozzolanic activity index test was also performed in Turkey Cement Manufacturers Research Laboratories located in Ankara/Turkiye in accordance with ASTM C989/989M-14 (2014) to evaluate the effect of the fineness on the pozzolanic properties (Table 2). For particle size distribution of the binders, wet dispersion method was also used since cement particles tend to agglomerate in dry state. Ethanol was used as dispersive medium in order to prevent the dissolution of the cement and slags particles and, ultrasound was also utilized during the PSD measurements. Slag has a glassy phase with some weak amorphous Ca-containing low peaks (Figure 1b). PSD and XRD profiles of the materials are given in Figure 1a,b.

**Table 2.** Chemical, mineralogical and physical properties of binders.

| Chemical composition (%) | OPC (%) | Slag (%) | Physical properties | OPC | Slag 3100 | Slag 4650 | Slag 6300 |
|---|---|---|---|---|---|---|---|
| $SiO_2$ | 19.10 | 40.24 | Specific gravity | 3.15 | 2.90 | 2.90 | 2.90 |
| $Al_2O_3$ | 5.35 | 11.68 | Specific surface ($cm^2/g$) | 4060 | 3100 | 4650 | 6300 |
| $Fe_2O_3$ | 3.45 | 0.66 | +90 µm sieve (%) | - | 0.8 | - | - |
| CaO | 62.29 | 36.63 | +45 µm sieve (%) | 2.64 | 12.3 | 3.85 | 0.62 |
| MgO | 0.95 | 5.90 | +32 µm sieve (%) | 7.11 | 24.6 | 8.33 | 2.78 |
| $TiO_2$ | 0.14 | 1.00 | Mineralogical | | | | |
| $Cr_2O_3$ | 0.007 | 0.006 | composition* | | | | |
| $Na_2O$ | 0.41 | 0.3 | $C_3S$ | 64.1 | - | - | - |
| $K_2O$ | 1.09 | 1.27 | $C_2S$ | 26.0 | - | - | - |
| MnO | 0.07 | 1.98 | $C_3A$ | 3.0 | - | - | - |
| $P_2O_5$ | 0.08 | 0.01 | $C_4AF$ | 3.7 | - | - | - |
| Loss on ignition | 1.53 | 0.9 | Basicity Index | - | | 0.96 | |
| $SO_3$ | 6.68 | 1.71 | Pozzolanic Index (%; 28 days) | - | 67.6 | 84.7 | 99.3 |

*: Mineralogical composition of the cement was determined under XRD Rietveld technique.

Liquid sodium silicate (LSS: 11.02% $Na_2O$, 22.1% $SiO_2$) was obtained from Ege chemicals Ltd. and Merck brand granular sodium hydroxide (SH:99.5%) were used as activators. Taking into account of the authors' previous studies, modulus ratio of sodium silicate (MS: mass ratio of $SiO_2$ to $Na_2O$) was set to 1.0 using SH while activator dosage was fixed at 8.0 wt.% of slag on dry basis.

### *2.2. Preparation of CPBs and strength tests*

CPB samples were prepared in four different recipes (Table 3) with ordinary Portland cement (OPC) and alkali-activated slags (AAS) having different specific surface areas (3100$cm^2/g$ (AAS-3100), 4650$cm^2/g$ (AAS-4600), 6300$cm^2/g$ (AAS-6300)). Binder dosage for CPB preparation was set to 7 wt.% on dry basis of total solids (tailings+binders).

**Table 3.** CPB design conditions.

| Binder Type | Binder content | Solid Content (%) | Water Content (%) | Water /Binder Ratio | Slump (inch) |
|---|---|---|---|---|---|
| AAS-3100 | 7% | 80.31 | 19.69 | 3.50 | 8.6 |
| AAS-4650 | 7% | 80.24 | 19.76 | 3.52 | 8.4 |
| AAS-6300 | 7% | 80.16 | 19.84 | 3,54 | 8.3 |
| OPC | 7% | 77.97 | 22.03 | 4.04 | 8.4 |

After mixing, fresh CPB materials at 8.5±0.2-inch slump height (~216 mm) measured according to ASTM C143/C143M-12 (2012) was poured into the plastic molds 54$^{mm}$ in diameter and 108$^{mm}$ in height with a perforated bottom for the drainage excess water. A total of 96 CPBs were produced for

 doi:10.20944/preprints202311.0116.v1



the experimental studies 72 of which were used during UPV, UCS, pH and sulphate monitoring at 14-28-56-112-224-360 days. Molds were sealed with plastic bags and put into a temperature-controlled curing cabinet having a humidifier at 20±1 °C and %85±1 humidity conditions. CPBs were subjected to UCS testing in accordance with ASTM C39/ C39M-14a (2014) using a 50 kN servo-controlled compression machine with a loading rate of 0.5 mm per minute. Tests were carried out on 3 CPBs at each curing time and average values were presented in the results. Strength and durability assessment were made considering 1.0 MPa threshold value suggested by Landriault (1995).

### *2.3. pH and sulphate monitoring*

pH and sulphate analyses were conducted on CPBs after UCS testing for the evaluation of acid and sulphate effects on the properties of CPBs. For pH and sulphate concentration measurements, the procedure suggested by Cihangir et al. (2012) was used. Initial pH and sulphate concentration of the tailings were 8.98 and 5712ppm, respectively. High sulphate concentration was attributed to the sulphate containing chemicals used and pyrite oxidations during the ore processing stages.

### *2.4. Microstructural Investigation*

Microstructural properties of CPBs produced using slags in three different specific surface area were aimed to investigate in this study, in detail. In this scope, detailed microstructural experimental studies were carried out under scanning electron microscope equipped with an energy dispersive X-ray spectroscopy (SEM+EDS) and mercury intrusion porosimeter (MIP). For microstructural studies, 24 additional CPBs were cast and used at 28-, 112- and 360-days curing only for these experiments. Obtained results were used to investigate the effect of slag fineness on the microstructural evolution of CPBs and the durability properties.

SEM+EDS studies were conducted at 15 kV accelerating voltage using a ZEISS-EVO MA-LS SERIES LEO 1550 SEM operated. EDS analyses were performed for phase definitions and determination of Ca/Si ratios at the corresponding curing periods to evaluate the acid and sulphate effects (Cihangir et al. 2018). Detailed procedures for sample preparation for SEM studies and Ca/Si determination can be found elsewhere (Cihangir and Akyol, 2018).

In order to investigate the relation between porosity and pore structure and the strength and durability properties of CPBs, porosity tests were carried out using a mercury intrusion porosimeter (MIP) under a Micromeritics AutoPore IV 9510 equipment based on ASTM D4404-10 (2010) on the samples at 28–112 and 360 days curing time. Details of the procedures for the preparation CPBs for MIP tests can be found elsewhere (Cihangir and Akyol, 2018). Obtained results of MIP tests were assessed in based on the International Union of Pure and Applied Chemistry (1972) classification.

### *2.5. Ultrasonic P-wave velocity testing*

Ultrasonic P-wave velocity (UPV) tests were performed on CPBs prior to UCS tests using a Portable Ultrasonic Non-destructive Digital Indicating Tester (PUNDIT Plus) according to ASTM C597-09 (2009). End surfaces of CPBs were flattened and the lengths of CPBs were measured within an accuracy of ±0.1 mm. Then, the surfaces were covered with a thin layer of gel in order to maintain a good contact between the transducers and CPBs. The transit time between the transducers (transmitter and receiver; 42 mm in diameter with 54 kHz) was measured in continuous mode. Details of the applied procedures for UPV testing can be found elsewhere Ercikdi et al. (2014). UPV values (UPVs) were calculated using the following equation and the mean UPVs were given in the results for each curing points.

$$UPV = x/t$$

where UPV is the P-wave velocity (m/s), x is the length between the transducers (m), and t is the travel time (μs).

Correlation tests were also carried out to investigate the relationship between the UCSs and UPVs using the predictive analytics software (PASW Statistics 18).

Preprints (www.preprints.org) | NOT PEER-REVIEWED | Posted: 2 November 2023 doi:10.20944/preprints202311.0116.v1



## 3. RESULTS and DISCUSSION

### *3.1. Effect of slag fineness on the strength evolution and durability properties of CPB*

Strength (UCS) evolution of CPB samples was given in Figure 2a. All CPBs provided the desired UCS at 28 days. Highest strength was obtained from AAS-6300 samples at 28 days while AAS-3100 samples produced the lowest values. UCS of OPC increased up to 56 days in a low rate and tended to decrease afterwards. The loss in strength after 112 days was about 30% considering 360-day strength dropping under the level of 14 days strength. Similar tendency in OPCs produced from sulphide rich tailings were obtained in the long-term in the previous studies by Cihangir and Akyol (2018) and Ercikdi et. al. 2009. The loss in strength of OPC-CPBs can be attributed to the high CaO content and the poor gel structure.

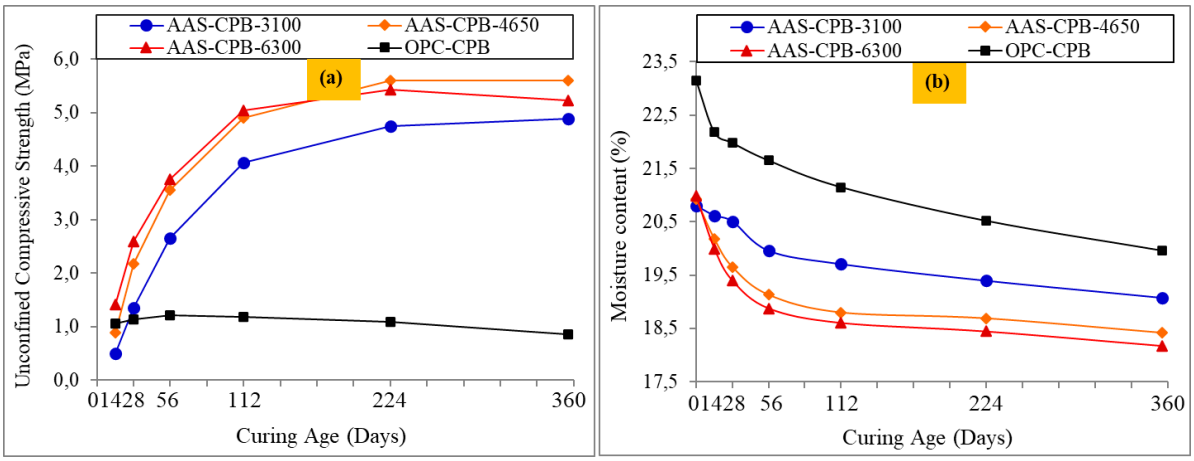


**Figure 2.** Effect of slag fineness on the UCS evolution (a) and variation of water/moisture content (b) of CPBs over the curing.

AAS-CPBs showed very high increasing trend and high slope in strength gain up to 112 days and displayed a slower increasing trend afterward. 360-days strengths of the AAS-3100, AAS-4650 and AAS-6300 series are 9.8-, 6.33 and 3.70-fold of the 14-days strength values, respectively. AAS-3100 samples produced lower strengths than those of AAS-4650 and AAS-6300 CPBs over the curing. Considering the average strength values of AASs over the curing, highest belonged to AAS-6300s. Average strength differences between AAS-3100, AAS-4650, AAS-6300 and OPC-CPBs are 3.03-, 3.78 and 3.91-fold, respectively. Similar strength differences when the slag fineness is about 4600 cm²/g were reached in previous studies performed on the sulphidic tailings CPB prepared with AAS in the long-term. On the other hand, the highest strength was obtained in case of AAS-4650 in the long term. AAS-CPBs showed relatively much better performance and resistance against aggressive environment than that of OPC (Shi et al. 2006; Cihangir et. al. 2015, Cihangir et al. 2018 and Cihangir and Akyol, 2018) except for AAS-6300 samples only where a 3.68% strength loss was observed after 224 days.

Hydration degree of the slag and its strength were reported to increase with increasing the Blaine fineness (Shi et al. 2006). The amount of <3μm slag fraction was found to provide higher early strength (Wan et.al. 2004). Besides, Wang et al. (2005) reached that <5μm of slag material amount significantly affected the hydration and 0-20 μm amount was crucial for early age (≤7days) strength development. However, they also found and reported that the amount of slag particles coarser than 20 μm decreased the reactivity of slag having less effect on early age strength gain. In the current study, <3μm fine particle amount of 6300 slag is ~2.5-fold of 3100 slag having 1.5-fold pozzolanic index value (Table 2). Therefore, AAS-3100 CPBs produced 1.78- and 2.83-fold lower strengths than those of AAS-4650 and AAS-6300 CPBs at 14 days. These results suggest that slag fineness and the amounts of fine fractions significantly affect the dissolution rate, amount of C-S-H gel products and, therefore, improvement of strength gain properties in AAS-CPBs.

Preprints (www.preprints.org) | NOT PEER-REVIEWED | Posted: 2 November 2023 doi:10.20944/preprints202311.0116.v1



Figure 2 also displays the moisture content of CPBs over the curing. Moisture content is at the lowest levels in AAS-6300 CPBs compared to those of others. In other words, the consumption of water seems to increase with the increase of the fineness of slag. This can be related to the continuous hydration/hydration product transformation etc. Shi et al. (2006) stated that the strength of the material may decrease due to the increase in water demand for slags whose fineness is over a certain value. Shi et al. (2006) also reported that further increase of the fineness from 5000 to 6000 $m^2/kg$ could cause a decrease in strength. According to Wang et al. (1994), proper strength development rates may be reached when the fineness of slag is in the range of 400 to 500 $m^2/kg$. The findings obtained from this study correspond very well with the related literature mentioned above.

*3.2. Effect of slag fineness on the pH and sulphate concentration evolution of CPBs*

Figure 3 depicts the pH and sulphate concentration levels of CPBs. pH values (pHs) of all CPBs displayed and increasing trend up to 14 days. The highest pHs belonged to OPC-CPBs up to 112 days which can be attributed to the hydration products such as C-S-H and $Ca(OH)_2$ (CH:Portlandite) (Lloyd et al. 2010). However, pH of OPC-CPBs tended to a drastic decline after 112-days and dropped under pH:10.4 at 360 days (Figure 3a) as an indication of the continuous oxidation of pyrite minerals (Cihangir et. al. 2015; Cihangir et al. 2018 and Cihangir and Akyol, 2018).

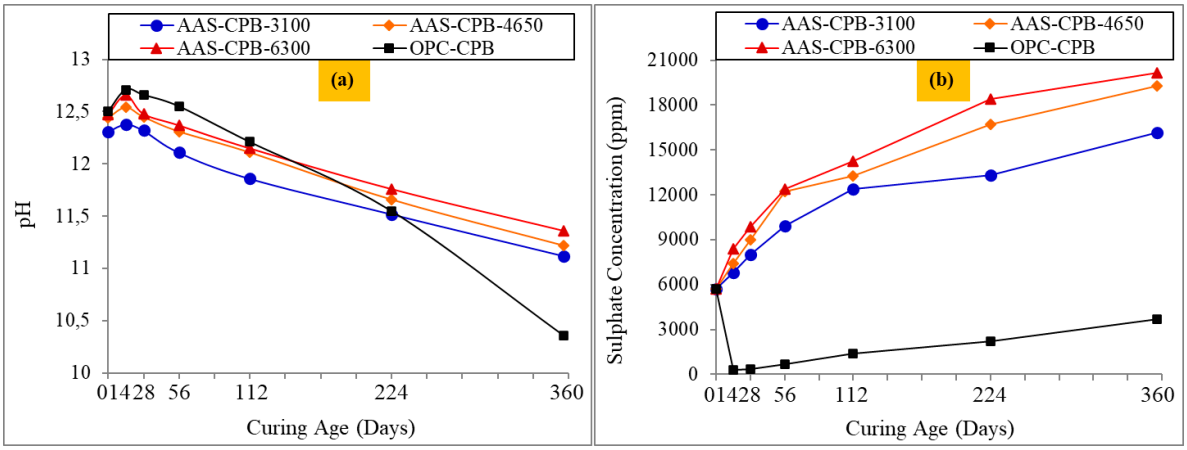


**Figure 3.** Effect of slag fineness on the pH and sulphate concentrate evolution of CPBs.

As for AAS-CPBs, pHs were measured to increase with the increase of slag fineness which can be related to the amount of higher dissolution rate and higher formation of hydration products with increasing the fineness of slag (Shi et al. 2006; Wang et al. 2005). CPBs with high slag fineness had high pHs during the curing. pHs of all AAS-CPBs stayed over pH:11.10 and the slope of decreasing trend is relatively very low compared to those of OPC-CPBs (Figure 3a). Similar results were obtained for pH levels of AAS-CPBs in the previous studies by Cihangir et. al. (2012), Cihangir et al. (2018) and Cihangir and Akyol (2018). Additionally, low early strength of AAS-3100 can be related to the lower pHs slowing down the hydration (Li et. al. 2019) during the very early ages.

Figure 3b demonstrates the sulphate evolution of CPBs over the curing. OPC-CPBs consumed the initial sulphate ions (Table 1) at early curing time which is the indication of sulphate attack. Poor strength gain rate in OPC-CPBs at the early ages can be ascribed to the sulphate ion adsorption into the gel products causing poor quality C-S-H. Additionally, lower sulphate ion concentrations were also the indication of sulphate attack forming expansive reaction products causing internal stress (Shi et. al. 2006) and disruption of OPC-CPB (Cihangir et al. 2012) resulting in strength loss in the long term.

On the other hand, AAS-CPBs with higher fineness had higher sulfate ion concentrations over the curing period as in pHs. It should be also noted here that the sulphate concentration of AAS-CPBs reached to ~16.000-20.000ppm which was thought to stem from high initial sulphate content of the tailings compares to the authors previous studies (Cihangir et. al. 2012; Cihangir et. al. 2018; Cihangir and Akyol, 2018). As the slag fineness increases, the consumption of sulphate ions seems to decrease.

Preprints (www.preprints.org) | NOT PEER-REVIEWED | Posted: 2 November 2023 doi:10.20944/preprints202311.0116.v1



This can be related to the formation of higher amount of C-S-H gels with low Ca/Si ratio precipitating on the particles in the CPB body acting a protective Si rich thick layer decreasing the rate of pyrite oxidation and consumption of sulphate ions, as well (Cihangir et. al. 2012).

*3.3. Influence of slag fineness on the microstructural evolution of CPBs*

Microstructural properties of CPBs were examined in detail together with the geochemical studies for both phase definition and Ca/Si ratio determination (Figure 4). Gel microstructure in OPC-CPBs has a fiber-like morphology at early curing ages (Figure 4a,b). Although the microstructure of OPCs looked dense at the early ages, it became loose as the curing time progressed. One of the reason stems from the lower solid content of OPC-CPB compared to those of AAS-CPBs (Table 3). Besides, the morphology tended to turn in a fiber-like/foil-like morphology which was ascribed to the continuous acid and sulphate effects with the elapse of curing time (Figure 4c). The bonding of C-S-H gels were observed to be weak to the tailings' particles. At 28 days, secondary gypsum like products were seen to integrate into C-S-H gels lowering the product quality, as well. In the SEM examinations performed on 28-day OPC sample, no obvious crystalline secondary gypsum was encountered although some small needle-like ettringite crystals were observed to form around the voids (Figure 4a,b). In the long term, obvious secondary gypsum products at different morphologies and coarse needle-like ettringite minerals were observed in OPC-CPBs (Figure 5). The authors related to the loss in strength to the acid and sulphate effects together with the secondary expansion minerals causing loose and heterogeneous microstructure (Fall and Benzaazoua, 2005; Ercikdi et. al. 2010; Cihangir et al. 2012; Cihangir et al. 2018, Cihangir and Akyol, 2018; Liu et. al. 2020).

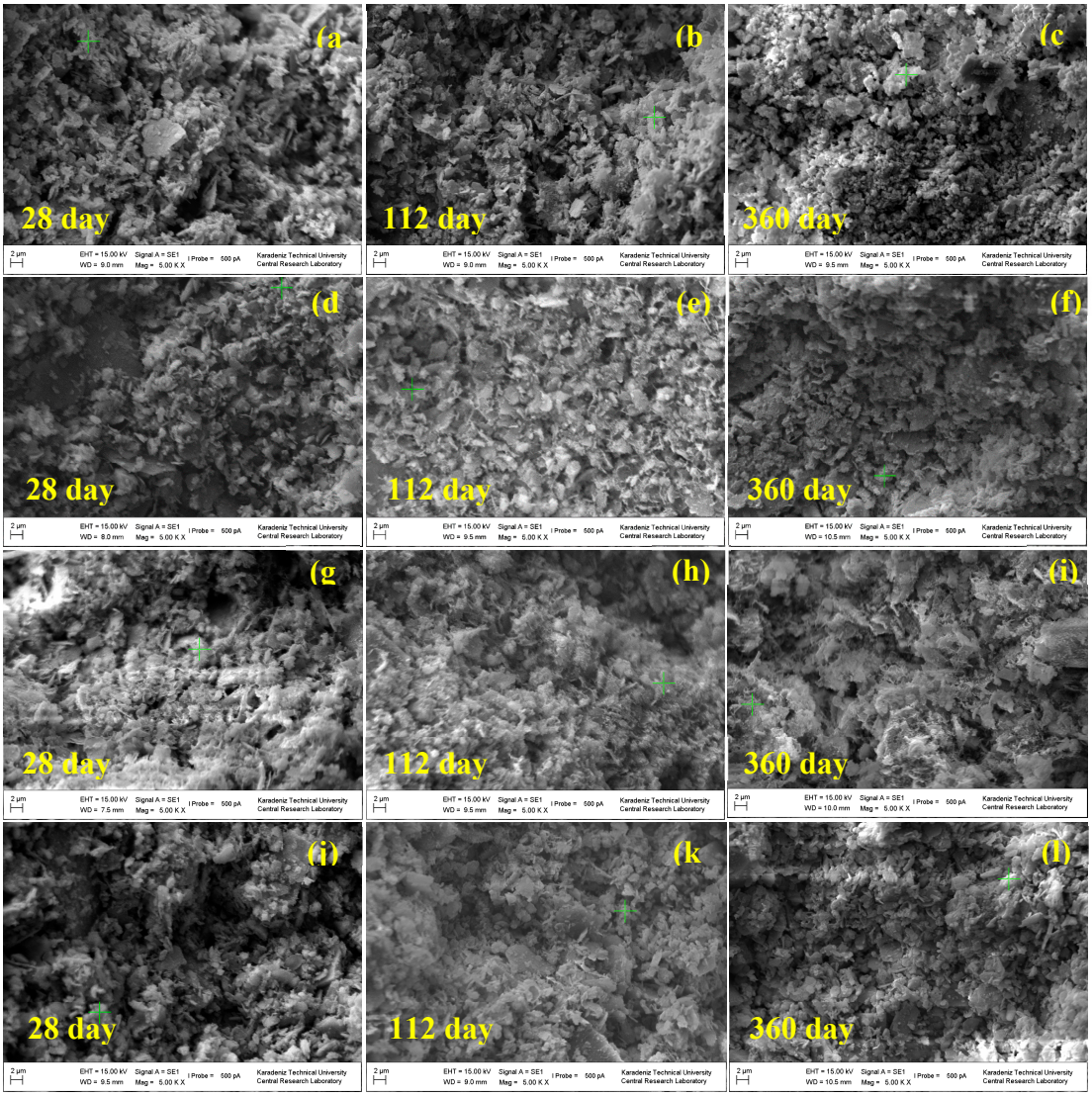

Preprints (www.preprints.org) | NOT PEER-REVIEWED | Posted: 2 November 2023 doi:10.20944/preprints202311.0116.v1



**Figure 4.** SEM images of OPC (a,b,c), AAS-3100 (d,e,f); AAS-4650 (g,h,i); AAS-6300 (j,k,l).

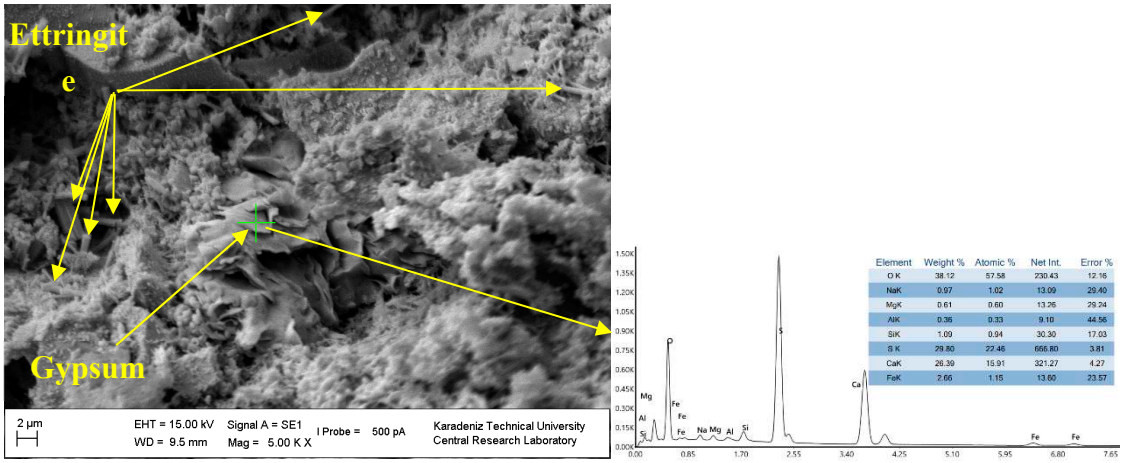


**Figure 5.** Secondary expansion mineral formations in OPC-CPB samples and their morphology.

As for AASs, all AAS-CPBs had a foil-like, gel-like (Figure 4d in AAS-3100 and Figure 4l in AAS-6300 samples), and denser microstructure compared to OPC-CPB. Foil-like hydration products were seen to cover most of the surfaces of the particles and the spaces between particles which can be related to the continuous strength gain in AASs. Voids between tailings particles were filled with the newly formed hydration products, with products transformed in other phases, and/or other secondary products such as gypsum, ettringite, monosulphate etc. with the elapse of curing time. The microstructure became denser and more compact in all AASs as the curing time increased. Among AASs, AAS-4650 had the densest foil-like structure especially at 112 days and at later ages while AAS-6300 sample had mostly gel-like morphology. Features/morphology of the C-S-H gel products can clearly be seen around the particles and the voids in AAS-CPBs (Figure 4 d-l).

During the SEM examinations and scanning, amount of secondary mineral phases was found to increase as the fineness of slag decreased at 112-days and later ages. Very well crystallized gypsum minerals having different morphologies and needle-like ettringites were observed to form in air bubbles (Figure 6) and voids as curing time proceeded to 112-days and thereafter. Secondary gypsum minerals were seen to form especially around and adjacent to pyrite minerals, and voids between tailings particles in all AASs where the most common and abundant formations were encountered in AAS-3100s during the SEM monitoring (Figures 7, 8 and 9b). Gypsum minerals looked finer and scattered in/around voids and within C-S-H gel products in AAS-6300 sample. Besides, hexagonal plate AFm (calcium sulphoaluminates/ monosulphoaluminate) phases were seen to be more common in AAS-6300s (Figure 4l).

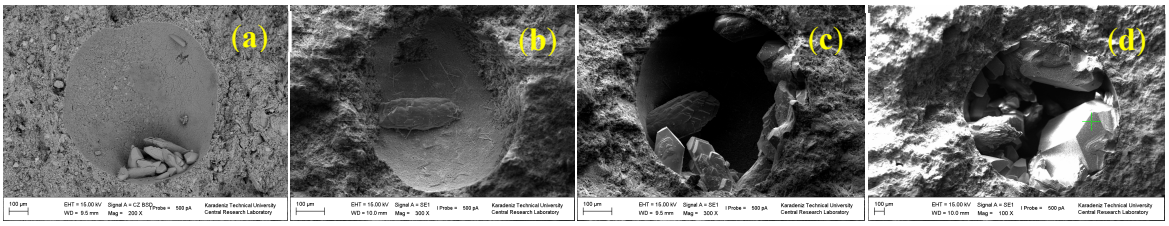


**Figure 6.** Secondary mineral formations in air bubbles in CPB body: gypsum in AAS-3100 (a), gypsum and ettringite in AAS-4650 (b), gypsum in AAS-4650 (c), gypsum in AAS-6300.

Preprints (www.preprints.org) | NOT PEER-REVIEWED | Posted: 2 November 2023 doi:10.20944/preprints202311.0116.v1



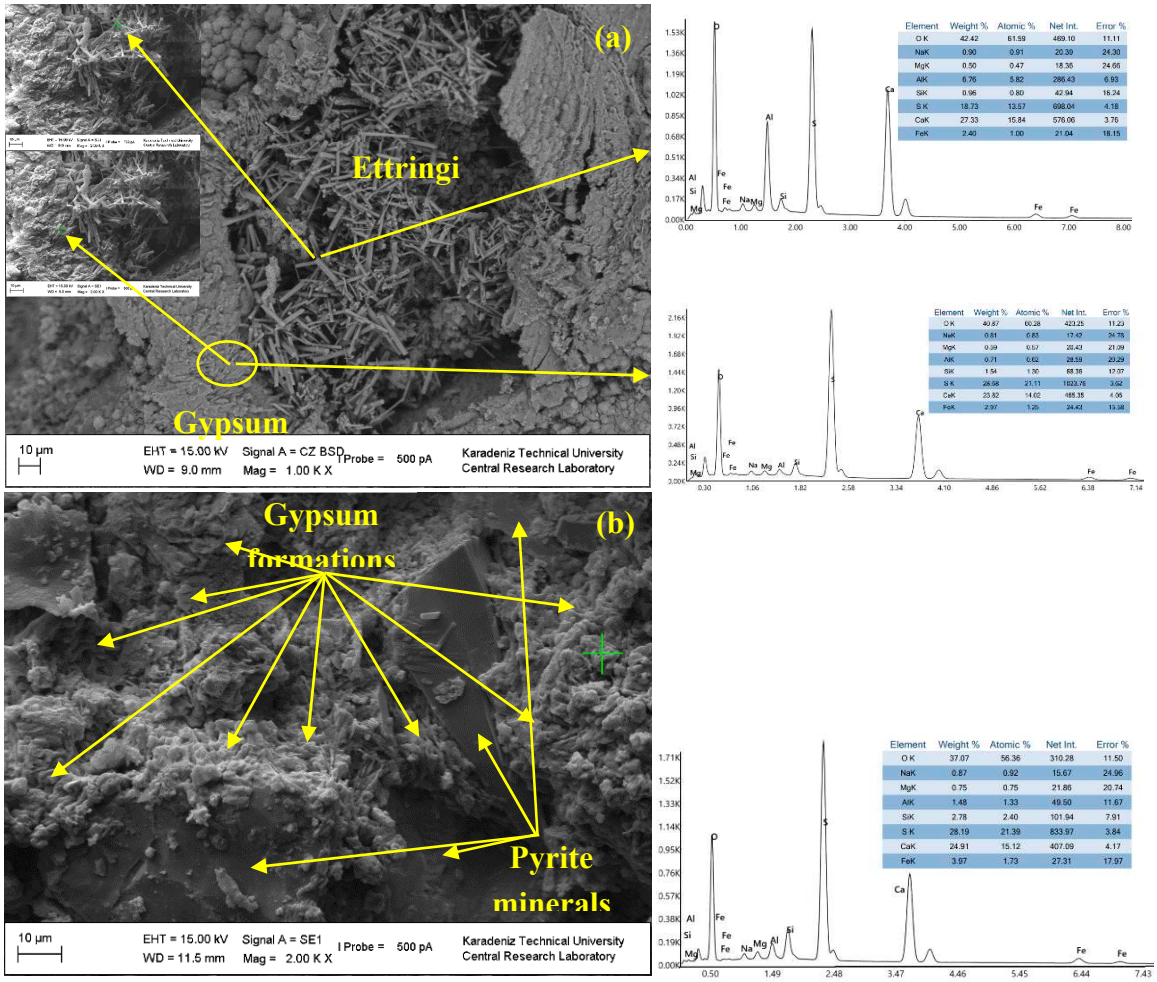


**Figure 7.** Secondary mineral formations in AAS-3100 at 360 days: ettringite (a), gypsum (b).

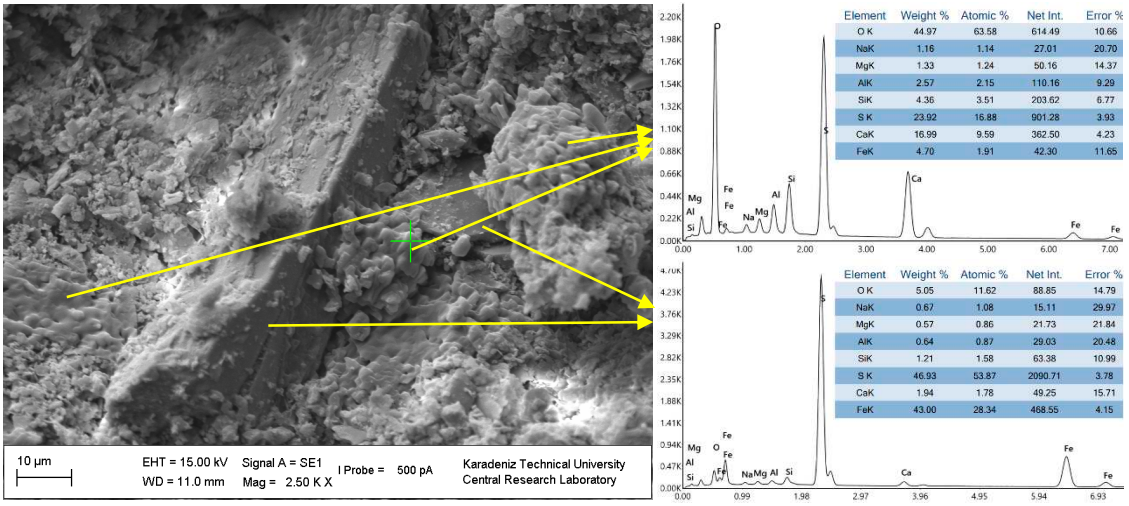


**Figure 8.** Secondary mineral formations around pyrite minerals in AAS-4650 at 360 days.

Preprints (www.preprints.org) | NOT PEER-REVIEWED | Posted: 2 November 2023 doi:10.20944/preprints202311.0116.v1



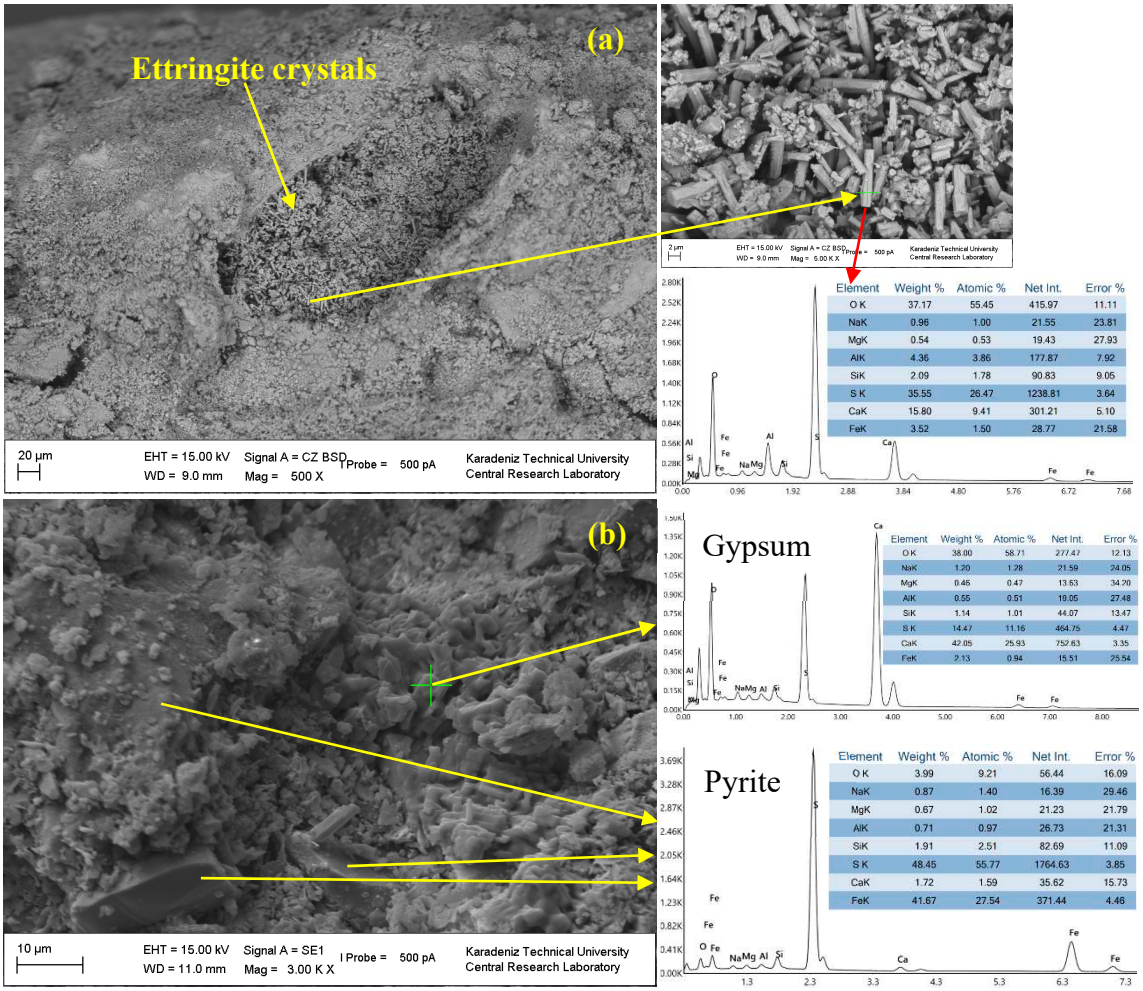


**Figure 9.** Secondary mineral formations (ettringite (a), gypsum (b)) in AAS-6300 at 360 days.

It should be noted here that needle-like ettringite minerals were detected within CPB material for the first time in this study in all AAS-CPBs. Coarser needle-like ettringites and ettringite clusters were found to form in air bubbles (Figures 6b, 7a and 9a) similar to gypsum crystal formations in such bubbles. The authors attribute this phenomenon to the very high initial sulphate ion content compared to the previous studies (Cihangir et al. 2012; Cihangir et al. 2015; Cihangir et al. 2018; Cihangir and Akyol, 2018) and the interaction of tailings with the binder agent (Benzaazoua et. al. 2004). Ettringite was reported to form when $Na_2SO_4$ was used as activator and/or sulphates were present in the medium (Shi et al. 2006).

Some drying shrinkage cracks were observed in AAS-6300 CPBs after 112 days (Figures 9a and 10). These cracks were thought to reason from the decrease in moisture content in AAS-6300 samples (Figure 2b). It is well-known that drying shrinkage is caused due to the moisture loss. A decrease in strength was reported to occur due to increase in water demand with increasing the fineness of slag. Additionally, drying shrinkage difference between AAS and OPC samples were reported to increase with the decrease in relative humidity (Shi et al. 2006). Therefore, the decrease in UCS of AAS-6300 sample in the long-terms can be related to such cracks.

Preprints (www.preprints.org) | NOT PEER-REVIEWED | Posted: 2 November 2023 doi:10.20944/preprints202311.0116.v1



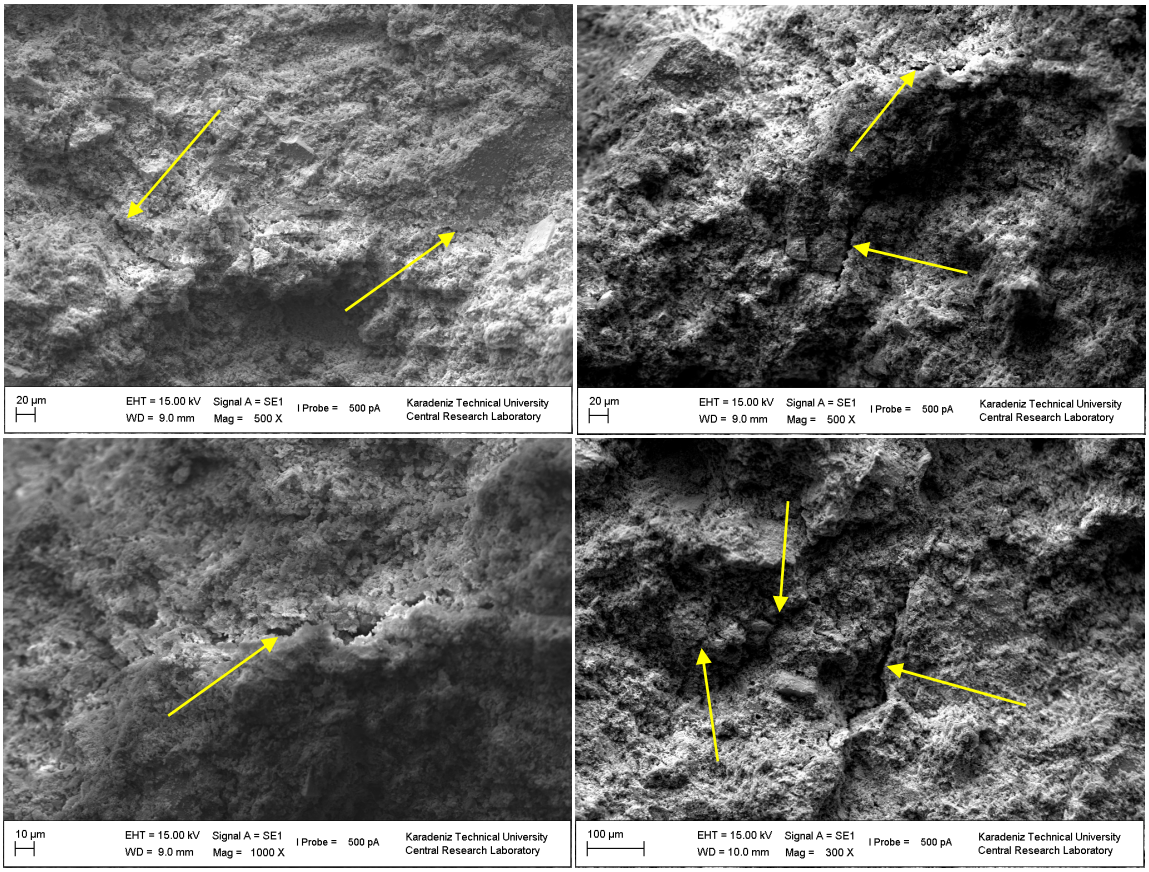


**Figure 10.** Crack formations in AAS-6300 CPB after 112 days.

Decalcification of C-S-H products depends on the drop in pH. With the decrease in pH C-S-H releases $Ca^{2+}$ ions for the neutralization of acid environment. Therefore, Ca/Si ratio of binding gel products were followed by spot chemical analysis under EDS to monitor decalcification and assess the durability properties of CPBs.

Ca/Si ratio of OPCs is 1.90 at 28 days which dropped to 0.89 at 360 days curing as an indication of continuous oxidation of pyrite minerals. Decreasing trend in Ca/Si ratio was high at the early stage which was ascribed to the high initial sulphate content consuming Ca products (dissolved $Ca^{2+}$ ions, etc.), and a bit dramatic after 112 days (Figure 11). Although Ca/Si ratio was 0.89 at 360-days, it looked like to fall even more. The poor strength performance of OPC-CPBs (Figure 2a) corresponds well with pH and sulphate ion change (Figure 3), loose microstructure (Figure 4b,c), and the change in Ca/Si ratios (Figure 11) with the elapse of curing time. The findings are in good agreement with the previous studies (Cihangir et al. 2018; Cihangir and Akyol, 2018). Decalcification is the most significant phenomenon for the durability performance of cemented materials compared to the expansive phases such as secondary gypsum, ettringite etc. (Komljenovic et al. 2013).

Preprints (www.preprints.org) | NOT PEER-REVIEWED | Posted: 2 November 2023 doi:10.20944/preprints202311.0116.v1



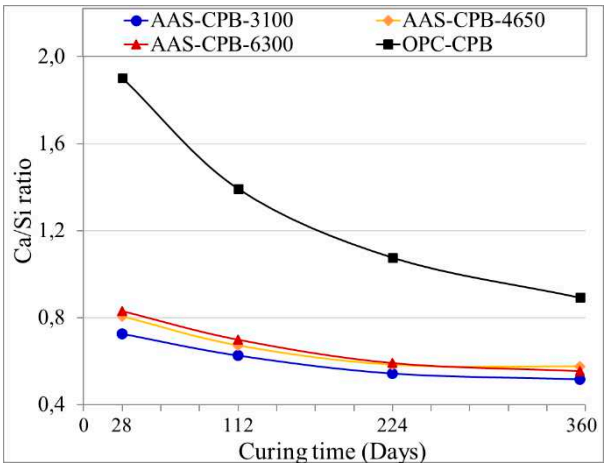


**Figure 11.** Ca/Si ratio of the binding gels of CPB samples.

Ca/Si ratios of the AAS-CPBs are less than those of OPC-CPBs due to the initial dissolved Si ions coming from the activator and the composition of slag of which Ca/Si ratio is ~0.91. The lowest Ca/Si ratios belonged to AAS-3100s over the curing. This can be related to the slower dissolution rate of coarser slag particles releasing less $Ca^{2+}$ ions, consumption of $Ca^{2+}$ ions for the formation of secondary expansive phases, and dissolved Si ions coming from the activator. Ca/Si ratios of AASs were about 0.8 at the early age and 0.55 at 360-days. The trends of decrease were much slighter compared to OPC-CPBs where trends were approximately parallel to the horizontal axis. This can be related to the outer Si rich protective C-S-H layer covering the surface of tailings particles and most importantly pyrite minerals reducing the oxidation (Cihangir et al. 2018; Cihangir and Akyol, 2018).

### *3.4. Pore size evolution of CPB samples*

Pore size distributions (PSD) and technical parameters of the curves of CPBs are seen in Figures 12 and 13, respectively. OPC-CPB sample has the highest total- and macro-porosities (macropores have pore size larger than 0.05 μm), and the lowest meso-porosities (mesopores range between 0.002 and 0.05 μm) (Iupac, 1972; Yilmaz et. al. 2011). For the given binder dosage, AASs have ~38% higher meso-porosity, while OPC-CPB sample has 18% and 10% higher macro- and total-porosities than those of AASs, respectively. Among AASs, 4650 sample has the finest pore structure considering the porosity curves although total porosity is not the lowest at all curing times (Figures 12 and 13a). At 360 days, pore size distribution curve of AAS-6300 sample was clearly seen to swell out/shift to right although the total porosity is approximately the same as other AASs (Figure 12b,d,f). Therefore, AAS-6300 has the highest macro porosity at 360 days. This phenomenon can be ascribed to the cracks formed due to the internal stress and/or drying shrinkage (Figure 10). This finding very well explains the low decrease in UCS in AAS-6300 CPB sample (Figure 2a).

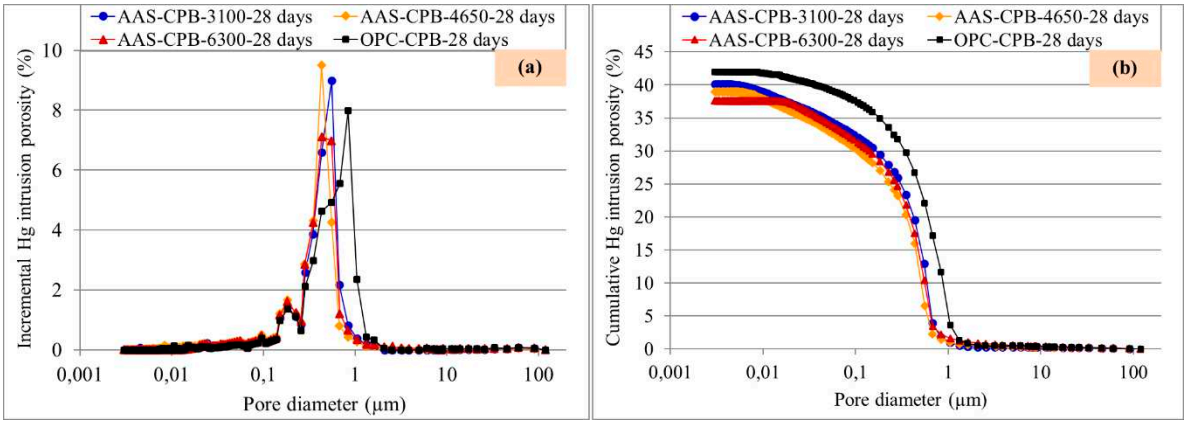

Preprints (www.preprints.org) | NOT PEER-REVIEWED | Posted: 2 November 2023 doi:10.20944/preprints202311.0116.v1



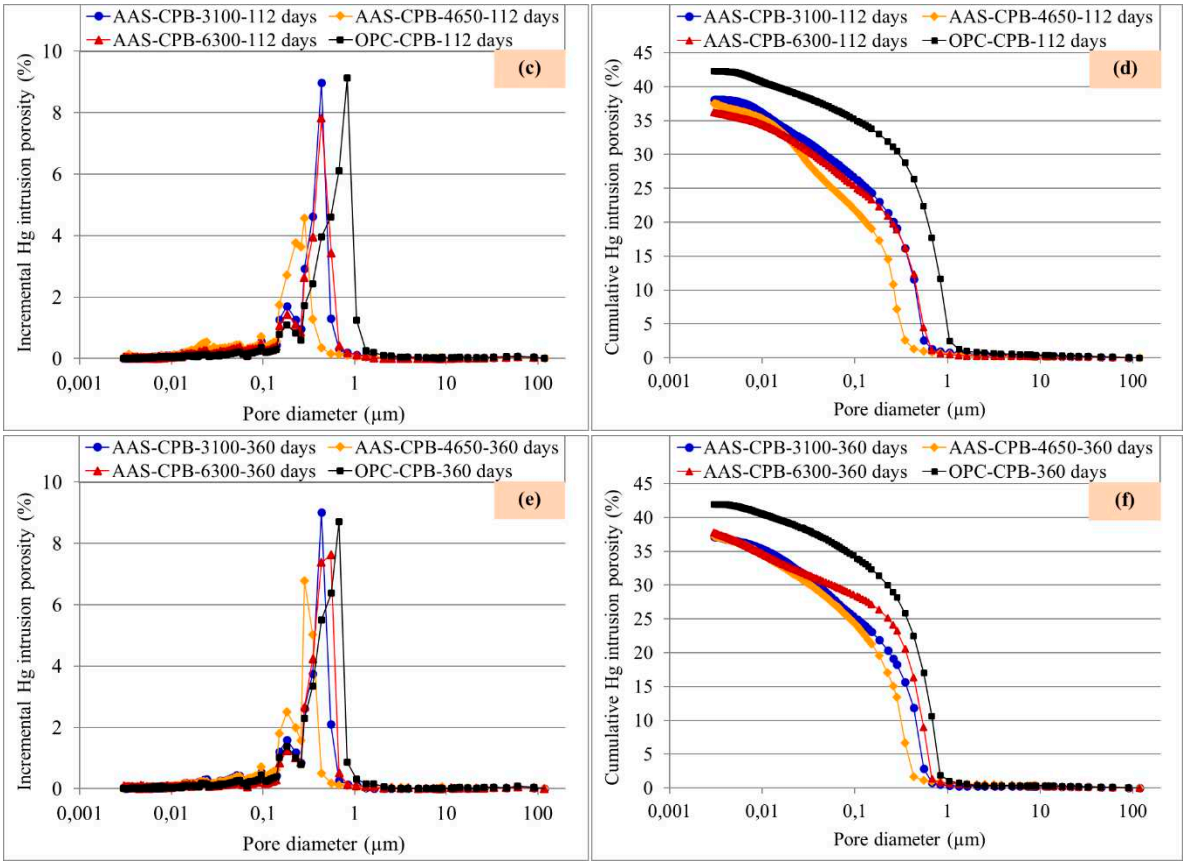


**Figure 12.** Incremental (a,c,e) and total (b,d,f) pore size distribution curves of CPB samples.

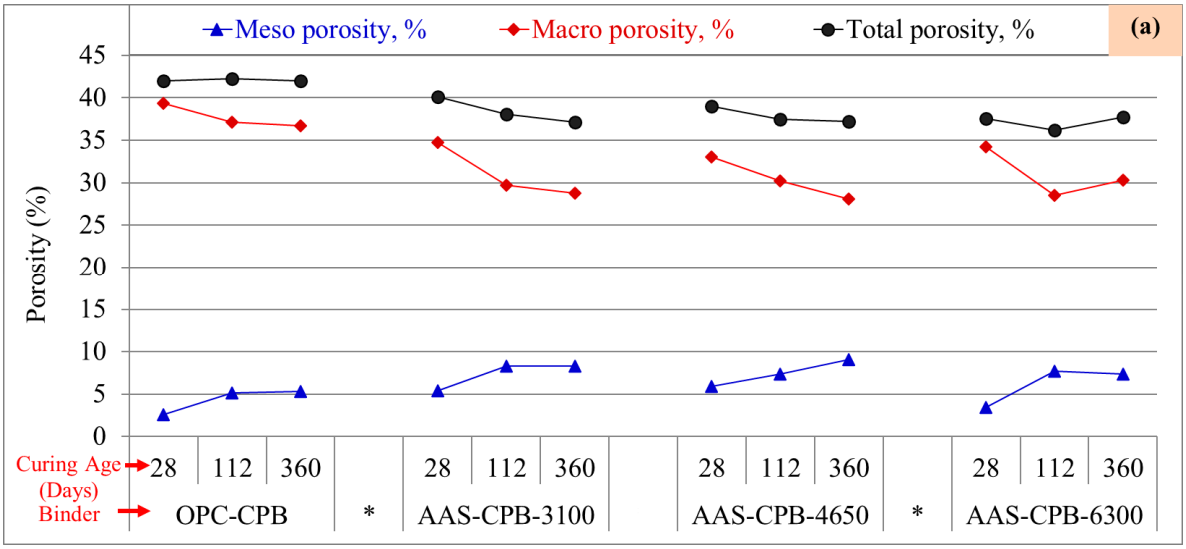

Preprints (www.preprints.org) | NOT PEER-REVIEWED | Posted: 2 November 2023 doi:10.20944/preprints202311.0116.v1



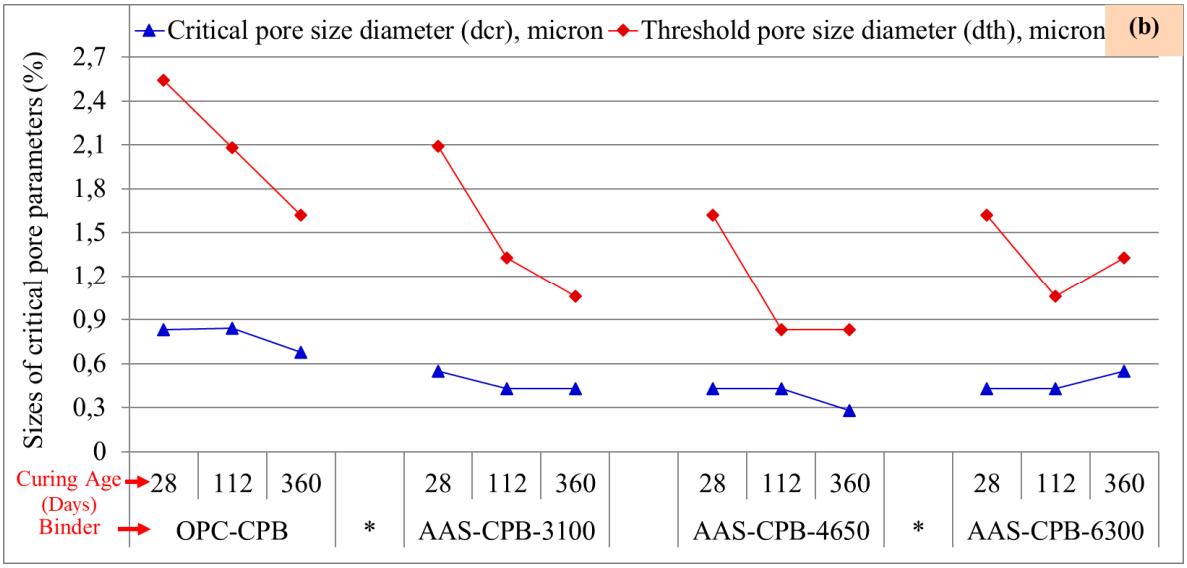


**Figure 13.** Technical parameters of the pore size distribution curves of CPB samples.

AAS-CPBs produced lower total porosities than those of OPC-CPBs in all curing times. Lower total porosities of AAS-CPBs can be related to the higher solids content at the preparation stage owing to the dispersant and lubricating effects of LSS and the newly formed C-S-H gels (Cihangir and Akyol, 2020).

For a given activator, total porosity and pore sizes were stated to become lower and finer, respectively, when the fineness of slag increases (Shi et al. 2006). In this study, evaluating together with the SEM images, the porous microstructure of the AAS-3100 and AAS-4650 samples were observed to become finer and denser with the progress of curing time which was more evident in AAS-3100 sample. Lower porosity and denser microstructure of these samples can be attributed to the continuous formation of C-S-H, other hydration products and, as well as secondary expansive minerals over the curing. It seems that formation of secondary expansive minerals (i.e., gypsum, ettringite) up to an amount had a beneficial effect on the decrease in porosity, improving the compactness (Figure 12) and resistance of AAS-CPBs against acid and sulphate effects (Shi et al. 2006; Fall et al. 2013).

On the other hand, $d_{cr}$ responsible for fluid transfer in CPB body is the highest in OPCs and the lowest in all curing times in AAS-4650s as can be seen from Figures 12a,c,e and 13b. As for $d_{th}$ (representing the largest pore diameters), OPCs had the coarsest pores at all curing times (Figures 12b,d,f and 13b). After 28 days, $d_{th}$ values were the lowest in AAS-4650 samples at all relevant curing times, and highest in AAS-6300 samples at 360 days among AAS-CPBs (Figures 12b,d,f and 13b) which is in line with the swelling of the AAS-6300 sample curve to the right.

Higher UCS and durability performance of AAS-CPBs can be related to the quality of binding gels, bond strength, impermeable, protective Si-rich gel products resistant to aggressive medium and porosity/PSD etc. (Shi et al. 2006; Komljenovic et al. 2013; Cihangir et al. 2018; Cihangir and Akyol, 2018). The findings clearly suggest that further increase in fineness of slag does not provide further advantage in terms of strength, microstructure and durability.

### *3.5. Evaluation of CPB strength and durability properties via P-wave velocity (UPV)*

Figure 14a depicts the ultrasonic P-wave velocity (UPV) propagation results of CPBs. Except for AAS-3100 and AAS-4650 samples at 14 days, UPV values (UPVs) of AAS-CPBs were higher than those of OPCs in all curing points. Lower UCS values for AAS-3100 and AAS-4650 samples at 14 days can be ascribed to the slower rate of strength development characteristics of the activated slags, and inhibitory effect of initial high sulphate ion concentration in CPB at very early ages (Cihangir et al. 2012; Cihangir et. al. 2018; Cihangir and Akyol, 2018; Meng et. al. 2023). UPVs of AASs were 1.15-, 1.22- and 1.23-fold in average for AAS-3100, AAS-4650 and AAS-6300 CPBs compared to OPCs,

Preprints (www.preprints.org) | NOT PEER-REVIEWED | Posted: 2 November 2023 doi:10.20944/preprints202311.0116.v1



respectively. Although AASs produced prominently greater UPVs than those of OPCs, the differences are very low compared to UCS values.

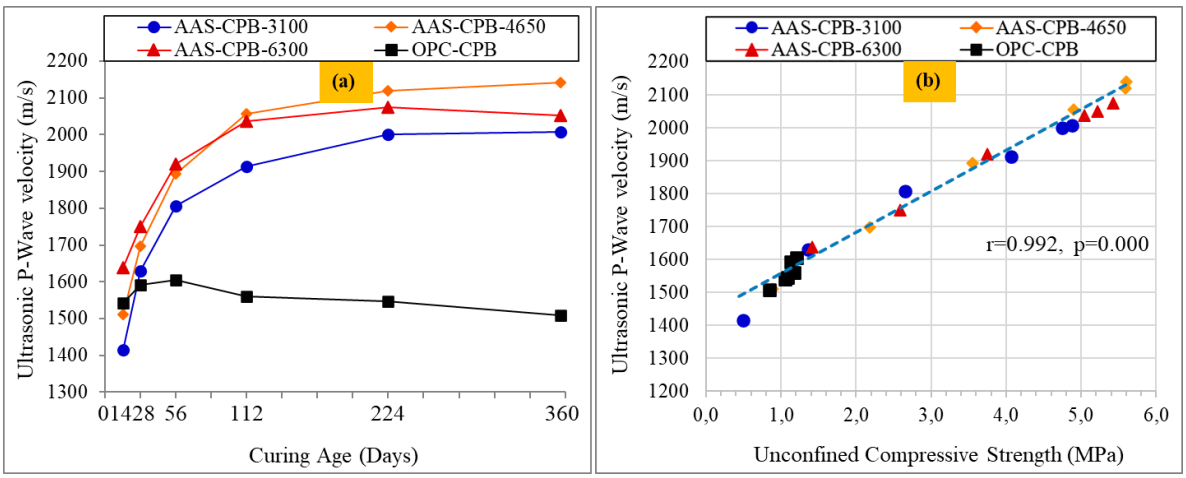


**Figure 14.** UPVs of CPBs during the curing (a) and the relation between UCS-UPV couples (b).

UPVs of AASs exhibited substantial growth trend for CPBs up to 112-day as a consequence of intensive formation, densification and solidification process of hydration products and slight rate of rise thereafter. These findings agree well with where similar trend was obtained between UPV and UCS couples in previous studies (Yilmaz et al. 2014; Cihangir, 2017). On the other hand, UPVs of OPCs displayed a decreasing trend after 56-days which was parallel to the UCS values. A decrease in UPV was also seen in AAS-6300 CPB as in UCS after 224-days. The loss in UPVs is associated with the *i)* acid productions causing decalcification-weathering-loosening in cemented matrix and so reduction in C-S-H bonds, and *ii)* sulphate productions resulting in disruption-disintegration and lowering the material stiffness due to the internal stress and an increase the heterogeneity in OPCs (Benzaazoua et. al. 1999; Ercikdi et. al. 2009; Cihangir et. al. 2012; Liu et. al. 2020). Besides, drying shrinkage cracks and possible detrimental secondary products are also responsible for the reduction in UPV of AAS-6300 after 224-days (Gaitero et al., 2008; Cihangir et. al. 2015; Cihangir, 2017; Cihangir et. al. 2018). Such structural imperfections lead to breakage and diffraction of UPV waves resulting in decrease (Gupta and Rao, 1998; Smolarkiewicz et. al. 2000; Aydın and Doven, 2006; Vasconcelos et. al. 2008).

Higher UPVs for AASs compared to OPCs can be related to the higher solids content, lower water/cement ratio (Table 3), resistance against acid and sulphate effects (Figure 3), compact microstructure (Figure 4), resistance of binding gels against decalcification (Figure 11), lower porosity and finer pore structure (Figures 12 and 13). Higher UPVs can also be attributed to the silicate polymerization, higher rate of solidification (Shi et al. 2006), quality of hydration products, and gain of strength in AAS-CPBs (Cihangir et al. 2012; Cihangir et. al. 2018; Cihangir and Akyol, 2018).

It is obvious that there is a similar trend of increase or decrease in UPVs and UCSs of CPBs at each corresponding curing point. The coefficient of correlation values between UCS and UPV couples of CPBs are very strong with "r" value of 0.992 (Figure 11). The direction of the relation is pozitive and the relation is significant between each couples within 95% confidence interval (Table 4). From this point of view, UPV measurements show that the strength and also the durability of CPBs can reliably and simply be followed and/or estimated for a specific CPB design for a mine operation.

 doi:10.20944/preprints202311.0116.v1



**Table 4.** Relationship between UCS and UPV couples of CPBs.

| Correlation parameters | Coefficient of Pearson correlation (r) | Sig. (2-tailed) |
|---|---|---|
| UCS-UPV for all CPB designs | 0.992 | 0.000 |
| UCS-UPV for AAS-3100 CPB samples | 0.982 | 0.001 |
| UCS-UPV for AAS-3100 CPB samples | 0.998 | 0.000 |
| UCS-UPV for AAS-3100 CPB samples | 0.997 | 0.000 |
| UCS-UPV for OPC-CPB samples | 0.872 | 0.023 |

## 4. Conclusions

According to the obtained results, AAS provides durable CPBs against acid and sulphate effects when CPB is made from sulphide rich tailings. In such medium, AAS can produce ~4-fold strengths compared to OPC in CPB.

Fineness of slag and fine fraction amounts were found to have influential effect on the dissolution rate and amount of hydration products formation affecting the improvement of strength gain properties in AAS-CPBs especially in the short term. Hydration product solidification was observed to slow down with decreasing the fineness of slag. Further increase in slag fineness was observed to have no more advantageous results in terms of UCS gain. On the contrary, it may have detrimental effects due to the drying shrinkage.

Abundant secondary gypsum and as well as ettringite minerals may form in case of high sulphate concentration and due to the continuous oxidation of pyrite minerals in CPB body. Increasing the fineness of slag was found to decrease secondary expansive mineral formations, but cause drying shrinkage cracks due to the excess moisture loss and/or water demand. The quality of C-S-H is very close in AAS-CPBs and displays similar resistance against aggressive environment.

Total porosity of AAS-CPBs decreased with increasing the slag fineness. However, the finest pore structure and most compact CPBs were reached in case of AAS-4650 slag. Secondary mineral formations up to an amount were seen to contribute to the decrease in porosity.

UPV was very sensitive to the defects and heterogeneity in CPB body and very effective tool for the evaluation of the durability of CPB.

Cumulative assessments of the mechanical, geochemical, microstructural and ultrasonic findings of this study suggest that around 4500 $cm^2/g$ slag fineness is sufficient for the preparation of AAS-CPB. Slag in this fineness appears to provide the early age strength desired for stability and the long-term strength required for durability of the CPB.

**Author Contributions:** Conceptualization, F.C., E.K.; methodology, F.C., E.K.; validation, F.C., E.K.; formal analysis, F.C., E.K; investigation, F.C., E.K.; resources, F.C., E.K; writing—original draft preparation, F.C., E.K; writing—review and editing, F.C., E.K; supervision, F.C.; project administration, F.C.; funding acquisition, F.C.; All authors have read and agreed to the published version of the manuscript.

**Funding:** The authors would like to acknowledge the financial support of The Scientific and Technological Research Institution of Turkiye (TUBİTAK) (Project No: 120M534).

**Data Availability Statement:** All the data that support the findings of this study are available from the corresponding author upon reasonable request.

**Conflicts of Interest:** The authors declare no competing interests.

## References

1. Altindag, R., 2012. Correlation between P- wave velocity and some mechanical properties for sedimentary rocks. J South African Inst Min nad Metullargy 112, 229–237.
2. Annor, A., Tarr, K., Fynn, D., 2006. Mechanical properties of a composite backfill material, proceedings of the core project on deep mining, Montreal-Canada, 128-137.
3. ASTM C39/C39M-14a, Standard test method for compressive strength of cylindrical concrete specimens, (2014). doi:http://dx.doi.org/10.1520/C0039.

4. ASTM D4404-10, Standard test method for determination of pore volume and pore volume distribution of soil and rock by mercury intrusion porosimetry, (2010). doi:http://dx.doi.org/10.1520/D4404-10.
5. Aydın, E., Doven, A.G., 2006. Influence of water content on ultrasonic pulse-echo measurements through high volume fly ash cement paste-Physicomechanical characterization. Res Nondestruct Eval. 17, 177–189.
6. Benzaazoua, M., Fall, M., Belem, T. 2004. A contribution to understanding the hardening process of cemented pastefill, Minerals Engineering, 17, 141–152. doi:http://dx.doi.org/10.1016/j.mineng.2003.10.022.
7. Benzaazoua, M., Ouellet, J., Servant, S., Newman P., Verburg, R., 1999. Cementitious backfill with high sulfur content: physical, chemical, and mineralogical characterization, Cement and Concrete Research, 29, 5, 719-725.
8. Chen, Q., Zhang, Q., Qi, C., Fourie, A. Xiao, C., 2018. Recycling phosphogypsum and construction demolition waste for cemented paste backfill and its environmental impact, Journal of Cleaner Production, 186, 418-429.
9. Chen, Q., Zhou, H., Wang, Y., Li, X., Zhang, Q., Feng, Y., Qi, C., 2022. Resistance Loss in Cemented Paste Backfill Pipelines: Effect of Inlet Velocity, Particle Mass Concentration, and Particle Size, Materials, 15, 3339. https://doi.org/10.3390/ma15093339
10. Chen, X., Shi, X., Zhou, J., Du, X., Chen, Q., Qiu, X., 2019. Effect of overflow tailings properties on cemented paste backfill, Journal of Environmental Management, 235, 133-144.
11. Christaras, B., 2009. P-wave velocity and quality of building materials, in: Proc. of the 3rd IASME/WSEAS Int. Conf. on Geology and Seismology (GES 2009). pp. 41–46.
12. Cihangir, F., Akyol, Y., 2018. Mechanical, hydrological and microstructural assessment of the durability of cemented paste backfill containing alkali-activated slag, International Journal of Mininig Reclamation and Environment, 32, 123–143.
13. Cihangir, F., Akyol, Y., 2020. Effect of desliming of tailings on the fresh and hardened properties of paste backfill made from alkali-activated slag, Advances in Materials Science and Engineering, 2020, 4536257, 1-11.
14. Cihangir, F., Ercikdi, B., Kesimal, A., Deveci, H., Erdemir, F., 2015. Paste backfill of high sulphide mill tailings using alkali-activated blast furnace slag: Effect of activator nature, concentration and slag properties, Miner. Eng. 83, 117–127, https://doi.org/10.1016/j.mineng.2015.08.022.
15. Cihangir, F., Ercikdi, B., Kesimal, A., Ocak, S., Akyol, Y., 2018. Effect of sodium-silicate activated slag at different silicate modulus on the strength and microstructural properties of full and coarse sulphidic tailings paste backfill, Construction and Building Materials, 185, 555–566.
16. Cihangir, F., Ercikdi, B., Kesimal, A., Turan, A., Deveci, H., 2012. Utilisation of alkali activated blast furnace slag in paste backfill of high-sulphide mill tailings: effect of binder type and dosage, Minerals Engineering, 30, 33–43.
17. Clayton, S., Grice, T., Boger, D.V., 2003. Analysis of the slump test for on-site yield stress measurement of mineral suspensions, International Journal of Mineral Processing, 70, 1-4, 3-21.
18. Ercikdi, B., Baki, H., İzki, M., 2013. Effect of desliming of sulphide-rich mill tailings on the long-term strength of cemented paste backfill, Journal of Environmental Management, 115, 5–13.
19. Ercikdi, B., Kesimal, A., Cihangir, F., Deveci, H., Alp, I., 2009a. Cemented paste backfill of sulphide-rich tailings: importance of binder type and dosage, Cement and Concrete Composites, 31, 268–274.
20. Ercikdi, B., Cihangir, F., Kesimal, A., Deveci, H., Alp, I., 2009b. Utilization of industrial waste products as pozzolanic material in cemented paste backfill of high sulphide mill tailings, Journal of Hazardous Materials, 168, 848–856.
21. Ercikdi, B., Cihangir, F., Kesimal, A., Deveci, H., Alp, I., 2010a. Utilization of water reducing admixtures in cemented paste backfill of sulphide-rich mill tailings. J. Hazard. Mater. 179, 940–946.
22. Ercikdi, B., Cihangir, F., Kesimal, A., Deveci, H., Alp, İ., 2010b. Effect of natural pozzolans as mineral admixture on the performance of cemented-paste backfill of sulphide-rich tailings. Waste Manag Res 28, 430–435.
23. Ercikdi, B., Yilmaz, T., Kulekci, G. 2014. Strength and ultrasonic properties of cemented paste backfill, Ultrasonics, 54 (1), 195-204.
24. Fall, M., Benzaazoua, M., 2005. Modeling the effect of sulphate on strength development of paste backfill and binder mixture optimization. Cem. Concr. Res. 35, 301–314.
25. Fall, M., Benzaazoua, M., Ouellet, S., 2005. Experimental characterization of the influence of tailings fineness and density on the quality of cemented paste backfill, Minerals Engineering, 18 (1), 41–44.

26. Gaitero, J.J., Campillo, I., Guerrero, A., 2008. Reduction of the calcium leaching rate of cement paste by addition of silica nanoparticles. Cem Concr Res 38, 1112–1118.
27. Gupta, A.S., Rao, K.S., Index properties of weathered rocks: inter-relationships and applicability, Bulletin Engineering Geology and Environment 57 (1998) 161–172.
28. Hamdi, E., Lafhaj, Z., 2013. Microcracking based rock classification using ultrasonic and porosity parameters and multivariate analysis methods. Eng Geol 167, 27–36.
29. IUPAC, Manual of symbols and terminology. Appendix 2-part 1: colloid and surface chemistry, J. Pure Appl. Chem. 31 (1972) 578–593.
30. Jiang, H., Han, J., Li, Y., Yilmaz, E., Sun, Q., Liu, J., 2020. Relationship between ultrasonic pulse velocity and uniaxial compressive strength for cemented paste backfill with alkali-activated slag, Nondestructive Testing and Evaluation, 35, 4, 359–377. https://doi.org/10.1080/10589759.2019.1679140
31. Jiang, H., Yia, H., Yilmaz, E., Liud, S., Qiu, J., 2020. Ultrasonic evaluation of strength properties of cemented paste backfill: Effects of mineral admixture and curing temperature, Ultrasonics, 100, 1-11, 105983.
32. Karaman, K., Kesimal, A., 2013. Kayaçların tek eksenli basınç dayanımı ile ultrasonik dalga hızı arasındaki ilişkinin değerlendirilmesi. MT Bilimsel, Yer Altı Kaynakları Derg 4, 9–17.
33. Karpuz, C., Pasamehmetoglu, A.G., 1997. Field characterisation of weathered Ankara andesites. Eng Geol 46, 1–17.
34. Kasap, T., Yilmaz, E., Guner, N.U., Sari, M., 2022. Recycling Dam Tailings as Cemented Mine Backfill: Mechanical and Geotechnical Properties, Hindawi, Advances in Materials Science and Engineering Volume 2022, 6993068, 1-12. https://doi.org/10.1155/2022/6993068
35. Kesimal, A., Erçıkdı, B., Yılmaz, E., 2003. The effect of desliming by sedimentation on paste backfill performance, minerals engineering, 16, 10, 1009-1011.
36. Kesimal, A., Yılmaz, E., Ercikdi, B., 2004. Evaluation of paste backfill test results obtained from different size slumps with varying cement contents for sulphur rich mill tailings. Cement and Concrete Research, 34 (10), 1817–1822.
37. Kilic, A., Teymen, A., 2008. Determination of mechanical properties of rocks using simple methods. Bull Eng Geol Environ 67, 237–244.
38. Koc, E., Cihangir, F., Ercikdi, B., Geochemical evaluation of sulfidic tailings and cemented paste backfill with respect to environmental impacts, Managing Mining and Minerals Processing Wastes: Concepts, Design, and Applications, In Eds: Chongchong Qi,Craig H. Benson, Elsevier Science, Oxford/Amsterdam , London, ss.47-70, 2023.
39. Komljenović, M., Baščarević, Z., Marjanović, N., Nikolić, V., 2013. External sulfate attack on alkali-activated slag, Construction and Building Materials, 49, 31–39. doi:http://dx.doi.org/10.1016/j.conbuildmat.2013.08.013.
40. Kou, Y., Jiang, H., Ren, L., Yilmaz, E., Li, Y., 2020. Rheological Properties of Cemented Paste Backfill with Alkali-Activated Slag, Minerals, 10, 288, 1-14. doi:10.3390/min10030288
41. Landriault, D.A. 1995. Paste backfill mix design for Canadian underground hard rock mining, in: Proceedings of the 97th Annual General Meeting of the CIM Rock Mechanics and Strata Control Session, Nova Scotia, Canada, 652–663.
42. Li, P., Tang, J., Chen, X., Bai, Y., and Li, Q., 2019. Effect of Temperature and pH on Early Hydration Rate and Apparent Activation Energy of Alkali-Activated Slag, Advances in Materials Science and Engineering, 2019, pp.13, https://doi.org/10.1155/2019/3531543.
43. Liu. L., Xin, J., Huan, C., Qi, C., Zhou, W., Song, KI-IL., 2020. Pore and strength characteristics of cemented paste backfill using sulphide tailings: Effect of sulphur content, Construction and Building Materials, 237, 117452, 1-13.
44. Lloyd, R.R., Provis, J.L., Van Deventer, J.S.J., 2010. Pore solution composition and alkali diffusion in inorganic polymer cement. Cem. Concr. Res. 40, 1386–1392.
45. Meng, J., Fall, M., Pour, H.M., 2023. Deeper Understanding of the Strength Evolution and Deformation Characteristics of Sodium Silicate–Cemented Paste Tailing Material, Minerals, 13, 1382, 1-28.
46. Pan, A., Grabinsky, M., 2023. Mechanical Characterization of Cemented Paste Backfill, Eng 2023, 4, 738–747. https://doi.org/10.3390/eng4010044
47. Pokharel, M., Fall, M., 2013. Combined influence of sulphate and temperature on the saturated hydraulic conductivity of hardened cemented paste backfill, Cement and Concrete Composites, 38, 21–28.

48. Qiu, J., uo, Z., Yang, L., Jiang, H., Zhao, Y., 2020. Effect of tailings fineness on flow, strength, ultrasonic and microstructure characteristics of cemented paste backfill, Construction and Building Materials, 263, 1-10, 120645.
49. Sari, M., Yilmaz, E., Kasap, T., Karasu, S., 2023. Exploring the link between ultrasonic and strength behavior of cementitious mine backfill by considering pore structure, Construction and Building Materials, 370, 1-18, 130588.
50. Shi, C., Krivenko, P.V., Roy, D. 2006. Alkali-Activated Cements and Concretes, Taylor and Francis, London.
51. Shuai, X., Fidelis, T.S., Lia, K., Li, Y., 2017. Evaluation of the strength and ultrasonic properties of foam-cemented paste backfill, International Journal of Mining, Reclamation and Environment, 31, 8, 544–557; https://doi.org/10.1080/17480930.2016.1215782
52. Smolarkiewicz, P.P., Nogueira, C.L., Willam, K.J., 2000. Ultrasonic Evaluation Damage in Heterogeneous Concrete Materials, in: European Congress on Computational Methods in Applied Sciences and Engineering (ECCOMAS 2000). Barcelona, pp. 1–13.
53. Vasconcelos, G., Lourenço, P.B., Alves, C.A.S., Pamplona, J., 2008. Ultrasonic evaluation of the physical and mechanical properties of granites. Ultrasonics 48, 453–466.
54. Wan, H., Shui, Z. ve Lin, Z., 2004, Analysis of Geometric Characteristics of GGBS Particles and Their Influences on Cement Properties, Cement and Concrete Research, 34, 1, 133–137.
55. Wang, P. Z., Trettin, R. ve Rudert, V., 2005. Effect of Fineness and Particle Size Distribution of Granulated Blast-Furnace Slag on the Hydraulic Reactivity in Cement Systems, Advances in Cement Research, 17, 4, 161-166.
56. Wang, S., Scrivener, K. L. and Pratt, P. L., 1994, Factors affecting the strength of alkali-activated slag. Cement and Concrete Research, 24(6), 1033–1043.
57. Wu, D., Zhao, R., Xie, C., Liu, S., 2020. Effect of curing humidity on performance of cemented paste backfill, International Journal of Minerals, Metallurgy and Materials, 27, 8, , 1046-1053. https://doi.org/10.1007/s12613-020-1970-y
58. Wu, D., Zhang, Y., Liu, Y., 2016. Mechanical performance and ultrasonic properties of cemented gangue backfill with admixture of fly ash, Ultrasonics, 64, 89–96.
59. Wu, J., Feng, M., Chen, Z., Mao, X., Han, G., Wang, Y., 2018. Particle Size Distribution Effects on the Strength Characteristic of Cemented Paste Backfill, Minerals, 8, 322; doi:10.3390/min8080322.
60. Xu, X., Sun, X., Yao, W., Wu, P., Qiu, J., Guo, Z., Liu, N., 2021. Strength and Ultrasonic Characteristics of Cemented Paste Backfill Incorporating Foaming Agent, Minerals, 11, 681, 1-18; https://doi.org/10.3390/min11070681
61. Xue, G., Yilmaz, E., Song, W., Cao, S., 2018. Compressive Strength Characteristics of Cemented Tailings Backfill with Alkali-Activated Slag, Applied Sciences, 8, 1537, 1-15. doi:10.3390/app8091537
62. Yan, B., Zhu, W., Hou, C., Yilmaz, E., Saadat, M., 2020. Characterization of early age behavior of cemented paste backfill through the magnitude and frequency spectrum of ultrasonic P-wave, Construction and Building Materials, 249, 1-12, 118733.
63. Yilmaz, E., Belem, T., Bussière, B., Benzaazoua, 2011. M. Relationships between microstructural properties and compressive strength of consolidated and unconsolidated cemented paste backfills, Cem. Concr. Compos. 33, pp. 702–715. doi:http://dx.doi.org/10.1016/j.cemconcomp.2011.03.013.
64. Yilmaz, T. Ercikdi, B., Karaman, K., Kulekci, G., 2014. Assessment of strength properties of cemented paste backfill by ultrasonic pulse velocity test, Ultrasonics, 54, 1386–1394.
65. Yilmaz, T., Ercikdi, B.., 2016. Predicting the uniaxial compressive strength of cemented paste backfill from ultrasonic pulse velocity test, Nondestructive Testing and Evaluation, 313, 247–266; http://dx.doi.org/10.1080/10589759.2015.1111891